Thickening mechanism under high compression stress based on rheological properties: Comparison between compression effect and compression-shear coupling effect

Aixiang Wu [1,2)], Zhenqi Wang [1*)], Zhuen Ruan [1,2,4*)], Raimund Bürger [3)], Shaoyong Wang [1,4)], Yi Mo [4,5)]

1) Key Laboratory of the Ministry of Education of China for High-efficient Mining and Safety of Metal Mines, University of Science and Technology Beijing, Beijing 100083, China

2) Shunde Innovation School, University of Science and Technology Beijing, Foshan 528399, China

3) CI^{2}MA and Departamento de Ingeniería Matemática, Facultad de Ciencias Físicas y Matemáticas, Universidad de Concepción, Casilla 160-C, Concepción, Chile

4) School of Civil and Resource Engineering, University of Science and Technology Beijing, Beijing 100083, China

5) China Railway Construction Tongguan Investment Co., Ltd, Tongling 244000, Anhui, China

*C**orresponding authors**: Zhenqi Wang, E-mail: 15101014530@163.com; Zhuen Ruan, E-mail: ustb_ruanzhuen@hotmail.com

Abstract: Tailings thickening is the primary link and key technology of cemented paste backfill (CPB) technology. However, the concentration of thickened tailings often is substandard because of the unclear of thickening mechanism. Therefore, this paper inveterated the thickening mechanism based on the rheological properties of tailings. Firstly, the double yield stress (compressive and shear yield stress) and concentration evolution under compression and compression-shear coupling effects were tested, respectively. And then the correlation analysis between concentration and double yield stress was carried out. The concentration shows a power function of the double yield stress, and shear yield stress is a linear function of the compressive yield stress. It is found that the linear fitting proportional coefficients under the compression effect are lower than those under the compression-shear coupling effect. The full compression stress range is divided into the low and high compression stress ranges and the shear yield stress-compressive yield stress proportional coefficients in the two compression stress ranges are linearly fitted. It is found that the proportional coefficients in the low compression stress range are lower than those in the high compression stress range under the compression effect, but the opposite results are shown under the compression-shear coupling effect, which shows that the introduction of rake-shearing action by the compression-shear coupling effect mainly improves the thickening rate and the thickening effect in the low compression stress range. Moreover, by introducing the rake-shearing action, the concentration growth ratio also confirms that the compression-shear coupling effect improves the thickening effect in the low compression stress range. Furthermore, from the evolution of

floc structure and drainage channels, the thickening mechanism of the compression effect and compression-shear coupling effect was revealed. The results are beneficial for obtaining a satisfied underflow concentration in CPB.

Keywords: High compression stress; Compression-shear coupling effect; Double yield stress; Concentration; Thickening mechanism

1 Introduction

The mining of metal mines causes many security factors, among which the tailings ponds and underground goafs are considered as the two major hazards [1-5]. Cemented paste backfill (CPB) technology is an environmentally friendly, safe, economical and high-efficient mining method that evenly mixes tailings, water and cementitious materials into paste slurry and then backfills it into the underground goafs. This method not only solves the problem of mining safety caused by underground goafs, but also eliminates the environmental pollution and land occupation of tailings ponds, and realizes the "one waste cures two evils" [6-10].

The process of CPB technology mainly includes tailings thickening, mixing, pipeline transportation (gravity or pumping), and stope maintenance, in which tailings thickening is the primary link and key technology. Tailings thickening thickens the low-concentration tailings slurry from the mill to form high-concentration paste-like underflow. The deep cone thickener (DCT) will output the high concentration tailings slurry through flocculation, sedimentation, compaction, and thickening in turn with its high-efficiency treatment capacity [15-22], and the thickening process of thickened tailings seriously restricts the throughput and thickening effect. Especially at present, the low ore grade and the mineral processing technology make the tailings particles processed from the mill develop in a finer and finer direction, which brings a series of problems such as difficult flocculation, turbid overflow, difficult thickening, and substandard concentration, which seriously restricts the development of thickening technology [23-25]. The concentration is the most important index to measure the thickening performance. The substandard concentration seriously affects the backfilling operations, which also harms the stability of the CPB structure and the backfilling cost.

The low concentration is mainly related to the thickening capacity of the thickener, and the thickening capacity depends on the thickener structure. The thickened tailings will show different thickening mechanisms with the different thickeners, further affecting the concentration. At present, thickeners mainly include ordinary thickener, high-efficiency thickener, and DCT (also called paste thickener) [26-29], among which DCT are widely used in CPB systems, and DCT is developed based on high-efficiency thickener, mainly to increase the compression stress of the thickened tailings and output higher concentration. The two most important factors in the DCT that affect the thickening are mud layer pressure and rake-shearing action. The mud layer pressure inside the DCT is mainly realized by increasing the mud layer height. The rake-shearing

action promotes the thickening through low-speed shearing effect, and whether or not the rake-shearing action greatly influences.

The research on the thickening mechanism of thickened tailings mainly focuses on the influence of mud layer height, rake-shearing rate, and other aspects. Still, it lacks the research from the angle of internal rheology. Rheology is an important basic theory of tailings thickening, and rheological properties are important internal factors of the concentration evolution. Among them, the thickened tailings of the thickener are under the high mud layer compression and the rake-shearing action, and it has the properties of compressive resistance and shearing resistance, showing the rheological properties of compressive yield stress and shear yield stress [30-37].

The research on thickening of thickened tailings mainly focuses on settling column tests and small-scale dynamic thickening simulation experiments [38-41]. These conventional indoor thickening experiments can only obtain concentration and rheological properties under the condition of low mud layer compression stress (<1 kPa), which is far from the high mud layer compression stress (5-100 kPa) of the industrial thickener, and has certain limitations on thickening mechanism. It is necessary to the thickening mechanism of thickened tailings with high compression stress.

The thickening process of thickened tailings is essentially a dynamic evolution process of flocs and drainage channels. A large number of studies have made micro-analysis (such as Computed Tomography (CT), Scanning Electron Microscope (SEM), and Focused Beam Reflectance Measurement (FBRM)) on tailings flocs and drainage channels, among which the theory of floc-shearing densification is put forward for the evolution of flocs under rake-shearing action [42-49]. Therefore, it is also necessary to investigate the thickening mechanism of thickened tailings from the perspective of the evolution of flocs and drainage channels.

In this study, the concentration and double yield stress evolution in the high compression stress (0-30 kPa) was tested by a self-developed compression-shear coupling experimental device, and the correlation between concentration and double yield stress was characterized, respectively. The thickening mechanism of thickened tailings was analyzed from the double yield stress relationship, concentration growth ratio, and the microscopic evolution of flocs and drainage channels.

2 Materials and methods

2.1 Raw materials

2.1.1 Tailings

The tailings used in this study come from a lead-zinc mine. The tailings are divided into classified tailings and fine-grained tailings by hydrocyclone. The unclassified tailings are composed of 30 wt% fine-grained tailings and 70 wt% classified tailings. The influencing factors of different fine-grained tailings contents are studied by changing the content of fine-grained tailings. Because the tailings particle size is ultra-fine, the fine-grained tailings and classified

tailings are analyzed by Omec Topsizer laser particle size analyzer [8,10]. The tailings particle size distribution and characteristic particle size of fine-grained tailings and classified tailings are shown in Fig. 1.

As can be seen from Figures 1(a) and 1(b), the particle size of fine-grained tailings is less than 100 μm, the particle size of tailings is in the range of 0.1-60 μm, the proportion less than 10 μm is more than 50 vol%, and the C_c (0.9) is less than 1, so it belongs to fine-grained tailings. The particle size of classified tailings is in the range of 1-400 μm, and the proportion of tailings larger than 100 μm is more than 30 vol%, and C_u is less than 5, so it belongs to coarse-grained tailings.

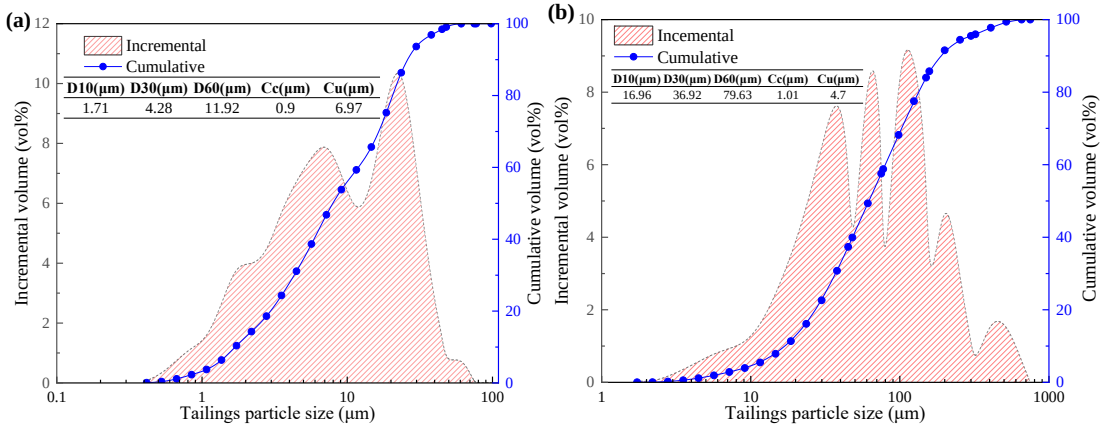

Fig. 1 Particle size distribution: (a) Fine-grained tailings; (b) Classified tailings

The specific gravity of fine-grained tailings and classified tailings was tested by the pycnometer method. The specific gravity of fine-grained tailings is 3.063, and that of classified tailings is 3.008. The porosity and specific surface area of fine-grained tailings and classified tailings were analyzed. The loose porosity of fine-grained tailings is 67.14%, the dense porosity is 59.09%, and the specific surface area is 1405.60 $m^2 \cdot kg^{-1}$. The loose porosity of classified tailings is 52.52%, the dense porosity is 40.16%, and the specific surface area is 172.86 $m^2 \cdot kg^{-1}$.

X-ray fluorescence (XRF) was used to analyze the main chemical composition of fine-grained tailings and classified tailings, and the analysis results are shown in Table 1. Both fine-grained tailings and classified tailings contain high contents of CaO and MgO, indicating that tailings contain more minerals, such as dolomite and calcite.

Table 1 Chemical composition of fine-grained tailings and classified tailings

	CaO	MgO	SiO2	Al2O3	Fe	S	Zn	Pb
Fine-grained tailings / wt%	38.62	6.63	6.17	2.8	2.29	2.02	1.05	0.96
Classified tailings / wt%	31.26	12.45	4.68	1.79	2.97	1.25	2.43	1.17

2.1.2 Flocculant and water

In this study, the flocculants suitable for tailings flocculation and thickening are selected, which are produced by SNF Company, including a cationic polyacrylamide (350E), a nonionic polyacrylamide (6003S) and three anionic

polyacrylamides (625S, 645th and 665S). The main difference among the three polyacrylamides is the different molecular weights, of which 665S is the highest, followed by 645S and 625S.

The flocculant was selected by settling column experiments. The feeding concentration of unclassified tailings is 15 wt%, the flocculant dosage is 20 g t^{-1}, and the flocculant dosage is 0.1 wt%. The height of the solid-liquid interface was recorded and the initial settling rate was obtained (0-60 s solid-liquid interface height fitted straight line slope). The initial settling rates corresponding to flocculant types 625S, 645S, 665S, 350E, and 6003S are 2.00 $mm \cdot s^{-1}$, 2.22 $mm \cdot s^{-1}$, 1.31 $mm \cdot s^{-1}$, 1.00 $mm \cdot s^{-1}$, and 1.34 $mm \cdot s^{-1}$, respectively. The concentration of the thickened tailings settled for 24 h was tested. The concentrations corresponding to 625S, 645S, 665S, 350E and 6003S are 44.40 wt%, 48.54 wt%, 38.61 wt%, 31.99 wt%, and 36.96 wt%, respectively, among which anionic polyacrylamide 645S has the highest initial settling rate and concentration, so anionic polyacrylamide 645S is selected as the flocculant used in the experiments.

The experimental water in this study is filtered tap water in the laboratory, and its pH is 7.0.

2.2 Experimental methods

These research experiments are divided into three stages, as shown in Fig. 2. Firstly, the flocculation condition optimization experiment was carried out, then the dynamic thickening experiment, and finally, the rheological properties and concentration under the compression and compression-shear coupling effects were tested.

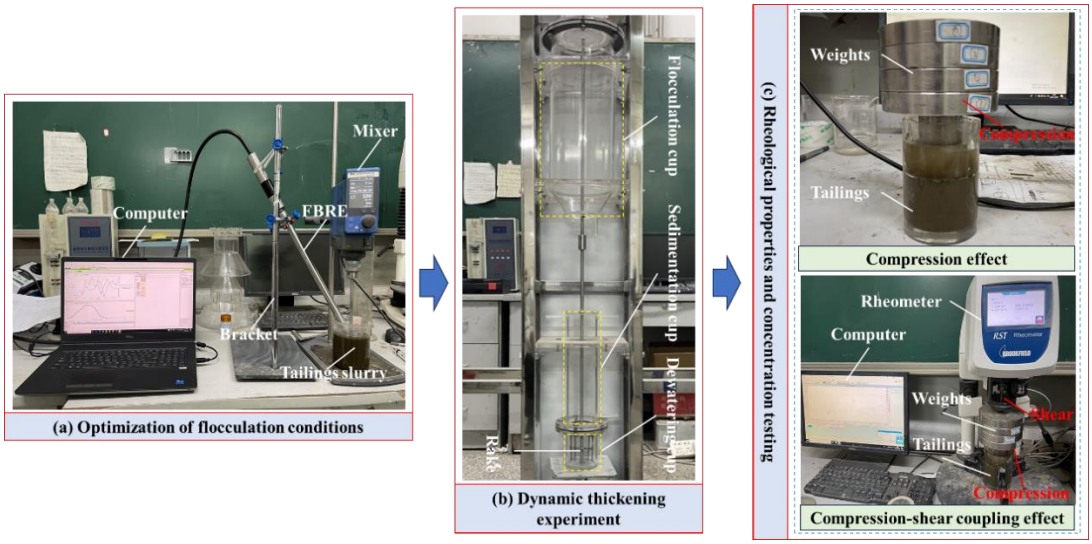

Fig. 2 Experimental procedure

2.2.1 Optimization experiment of flocculation conditions

As shown in Fig. 2(a), the mean weighted chord length (MWCL) of flocs in the flocculation process was tested using this experimental device, and the sedimentation characteristics were studied to obtain the concentration under different flocculation conditions. The experiment(a) adopted the Box-Benhnken Design (BBD) experimental method. Taking tailings feeding concentration,

flocculant solution concentration, shear rate, and shear time as experimental factors, the tailings feeding concentration range is 10-25 wt%, flocculant solution concentration range is 1-10 wt‰, shear rate range is 80-400 $r \cdot min^{-1}$ and shear time range is 30-150 s. The time-ending MWCL and concentration were taken as the response values to optimize the flocculation conditions, and there were 29 experimental groups (the experimental scheme is shown in Table 2). The specific experimental process is as follows:

(1) Tailings slurry was prepared according to the experimental scheme in Table 2. The mixer (IKA EUROSTAR 60 digital) was used for shearing at the specified speed, and then the tailings floc size evolution was tested by FBRM. In this study, the portable Particle Track G400 testing device was used for data collection and transformation with iC FBRM software, and the sampling period was set to 2s to test the tailings floc size evolution within the specified shearing time.

(2) Put the tailings slurry tested by FBRM into a 1000 ml measuring cylinder for settling column experiments. After settling for 24 h, test the concentration of different experimental groups.

The MWCL and concentration corresponding to different experimental groups shown in Table 2 are finally obtained through the above experiments. The optimal flocculation conditions are obtained using the “Optimization” function in Design Expert software, with the maximum concentration and MWCL as the goals. Finally, the optimal flocculation conditions are as follows: tailings feeding concentration is 17.05 wt%, flocculant solution concentration is 1.00 wt‰, shear rate is 166.11 $r \cdot min^{-1}$, and shear time is 30 s. Under these optimal conditions, the theoretical concentration is 58.48 wt%, and the MWCL of the floc is 299.694 μm.

Table 2 Flocculation conditions optimization experimental scheme and results

No.	TFC (wt%)	FSC (wt‰)	SR ($r \cdot min^{-1}$)	ST (s)	MWCL (μm)	Concentration (wt%)
1	25	5.5	400	90	32.123	35.8254
2	17.5	1	400	90	106.831	44.0545
3	17.5	5.5	240	90	236.357	45.1704
4	10	5.5	400	90	187.602	51.1485
5	17.5	10	400	90	121.315	43.9588
6	17.5	10	240	150	202.028	49.4854
7	10	10	240	90	251.134	59.5803
8	17.5	5.5	240	90	236.357	45.1742
9	10	1	240	90	185.378	54.4317
10	17.5	5.5	240	90	236.357	45.1742
11	17.5	5.5	400	150	94.608	40.2739
12	17.5	5.5	80	150	132.971	52.8526
13	25	5.5	80	90	134.008	43.6431
14	17.5	5.5	240	90	236.357	45.1742
15	10	5.5	80	90	128.945	56.0921
16	17.5	10	80	90	118.342	50.0475

17	10	5.5	240	150	99.303	54.7166
18	25	10	240	90	71.185	33.7223
19	25	5.5	240	150	84.825	36.1826
20	17.5	1	240	150	144.761	46.4598
21	17.5	1	80	90	182.309	55.0657
22	17.5	1	240	30	302.471	56.3792
23	17.5	10	240	30	226.213	45.2413
24	10	5.5	240	30	278.657	55.548
25	17.5	5.5	400	30	209.042	46.2535
26	17.5	5.5	240	90	236.357	45.1742
27	25	1	240	90	150.314	47.6158
28	25	5.5	240	30	195.722	44.9131
29	17.5	5.5	80	30	207.708	52.3361
Optimal results	17.05	1.00	166.11	30	299.694	58.4800

2.2.2 Dynamic thickening experiment

As shown in Fig. 2(b), a three-stage dynamic flocculation thickening experimental device was used to carry out the dynamic thickening experiment. The experimental device consists of a flocculation cup, sedimentation cup and thickening cup from top to bottom, and the concentration is improved by the rake shearing at low speed. The device was used to carry out dynamic thickening experiments under different flocculant dosages and fine-grained tailings contents to obtain high-concentration underflow and provide raw materials for rheological properties and concentration tests. Among them, the flocculant dosage levels are 10, 15, 20, 25, and 30 g t^{-1}, and the fine-grained tailings content is realized by changing the content of fine-grained tailings, which is divided into five levels: 10, 20, 30, 40, and 50 wt%. Other experimental conditions are carried out with the optimal flocculation conditions obtained in section 2.2.1. The experimental scheme of the dynamic thickening experiment is shown in Table 3.

Table 3 Experimental scheme of the dynamic thickening experiment

TFC (wt%)	FSC (wt‰)	SR ($r \cdot min^{-1}$)	ST (s)	Flocculant dosage (g t^{-1})	Fine-grained tailings content (wt%)
17	1	167	30	20	10, 20, 30, 40, 50
17	1	167	30	10, 15, 20, 25, 30	30

2.2.3 Rheological properties and concentration test

The traditional indoor settling column experiment and small-scale dynamic thickening experiment can only study the thickening behavior of thickened tailings under low compression stress (<1 kPa) [11,17,19], and there is a lack of research on rheological properties and concentration of thickened tailings during thickening under high compression stress and rake-shearing action. Therefore, in this study, the concentration and rheological properties of thickened tailings under compression and compression-shear coupling effects with high compression stress were studied.

As shown in Fig. 2(c), in this experiment, the rheological properties and concentration tests of thickened tailings obtained by the dynamic thickening

experiment in Fig. 2(b) were tested under the effects of compression and compression-shear coupling, respectively (Fig. 3), and finally, the compressive yield stress, shear yield stress and concentration evolution under different flocculant dosages and fine-grained tailings contents were tested. The main difference between the compression effect and compression-shear coupling effect is whether there is a low-speed rake-shearing action. This experiment also lays a physical foundation for revealing the rake-shearing thickening mechanism.

(a) Compression effect

As shown in Fig. 3(a), the compression effect mainly simulates the thickening behavior of the thickened tailings (high mud layer pressure in the DCT) of the rakeless DCT. The overlying compression stress of the thickened tailings is increased by increasing weights. The weights are made of stainless steel, and the weight sleeve controls the weights to keep the vertical state. Under the weights, there are bearing plate (acrylic material with holes), filter layer (EPE), and filter paper (Whatman Grade2 medium-speed), and the gravity of the weights is equivalent to compressive yield stress. Five pressure levels (C1: 2.55 kPa; C2: 8.66 kPa; C3: 14.78 kPa; C4: 20.89 kPa; C5: 27 kPa), each compression stress level is applied for 30 min, the seepage water is sucked out and weighed in time, the concentration of each compression stress level is calculated, and the shear yield stress corresponding to each compression stress level is tested by Brookfield R/S plus rheometer (CSR testing method: 0~120 s: 0~120 s^{-1}; 120~240 s: 120~0 s^{-1}).

(b) Compression-shear coupling effect

As shown in Fig. 3(b), the compression-shear coupling effect mainly simulates the dewatering behavior of the thickened tailings of the DCT with rake-shearing action. Compression stress is applied to the thickened tailings by the weights, and rake-shearing action is applied to the tailings slurry by the vane spindle (VT-40-20) of the rheometer to realize the coupling effect of compression and rake shearing. The shear rate of the vane is 2 $r \cdot min^{-1}$, and the compression stress testing procedure is the same as above. Finally, concentration and rheological properties can be obtained.

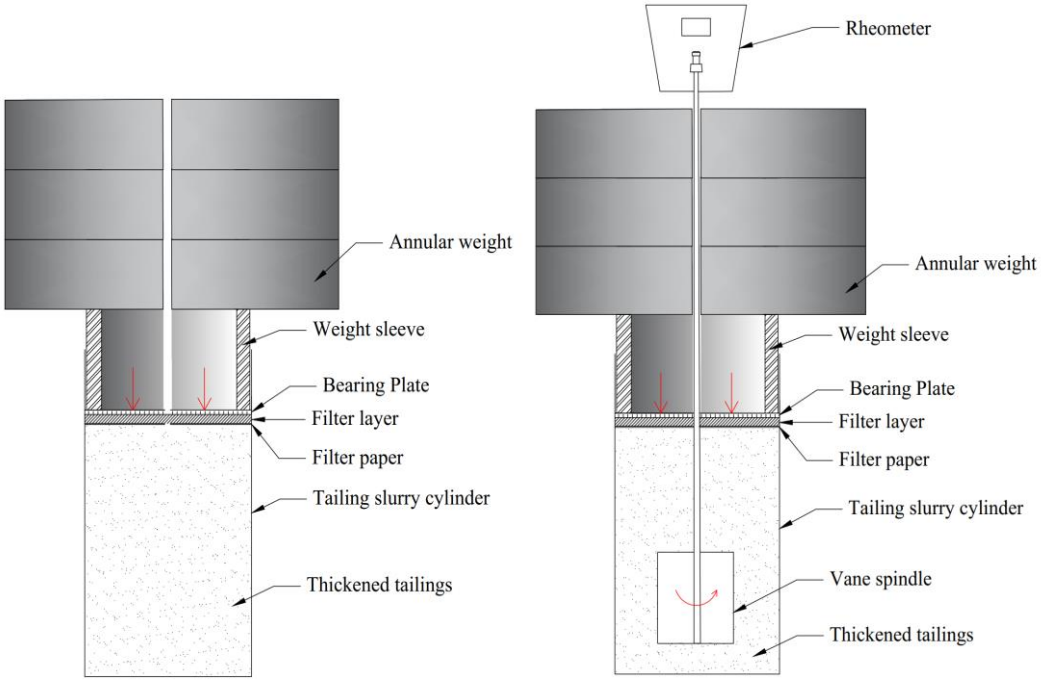

(a) Compression effect (b)Compression-shear coupling effect

Fig. 3 Rheological properties and concentration testing device

3 Results and discussion

3.1 Evolution of concentration and rheological properties

3.1.1 Evolution of concentration and rheological properties with different flocculant dosages

The concentration-double yield stress evolution under compression effect with different flocculant dosages is shown in Fig. 4. The concentrations of different flocculant dosages increase rapidly at first and then slow down with the linear growth of compressive yield stress, and the growth rate (5.89, 4.68, 4.64, 2.26, 3.83 %·kPa^{-1}) is higher in the low compressive yield stress range (0-2.55 kPa) than that (0.63, 0.58, 0.62, 0.71, 0.50 %·kPa^{-1}) in the high compressive yield stress range (2.55-27 kPa). The maximum concentration corresponding to the maximum compressive yield stress (27 kPa) is 69.47 wt% (flocculant dosage is 10 g t^{-1}). The shear yield stress shows a linear growth trend with increased compressive yield stress. The maximum shear yield stress is 302.81 Pa (flocculant dosage is 25 g t^{-1}), and the concentration also shows a trend of rapid growth at first and then slow with the increase of shear yield stress.

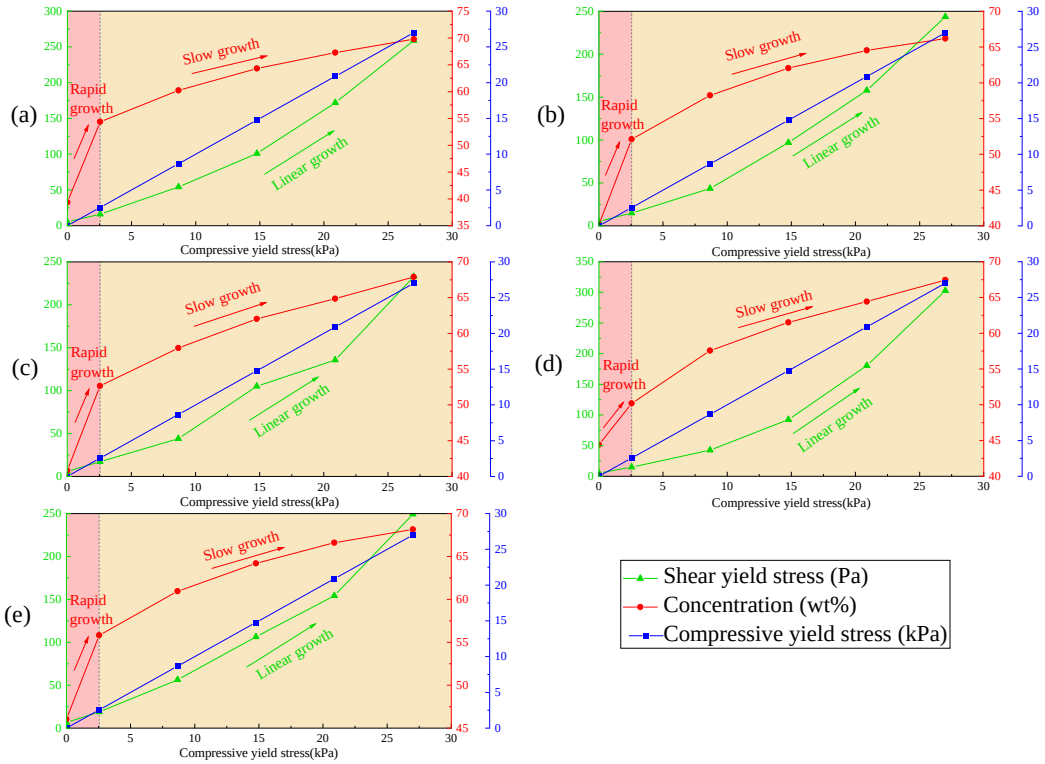

Fig. 4 Evolution of concentration-double yield stress under compression effect with different flocculant dosages: (a) 10 g t^{-1}; (b) 15 g t^{-1}; (c) 20 g t^{-1}; (d) 25 g t^{-1}; (e) 30 g t^{-1}

Fig. 5 shows the evolution of the concentration-double yield stress under the compression-shear coupling effect with different flocculant dosages. The concentrations of different flocculant dosages increase rapidly at first and then slow down with the linear growth of compressive yield stress. The growth rate (6.81, 6.04, 6.59, 4.08, and 5.60 %·kPa^{-1}) is higher in the low compressive yield stress range than that in the high compressive yield stress range (0.57, 0.57, 0.52, 0.56, 0.44 %·kPa^{-1}). Moreover, the concentration growth rate in the low compressive yield stress range under compression-shear coupling effect is higher than that under the compression effect, but in the high compressive yield stress range, the opposite is true. The maximum concentration is 71.18 wt% (flocculant dosage is 30 g t^{-1}), and the concentration is greatly improved compared with the compression effect, which shows that the thickening effect under the compression-shear coupling effect is better than that under the compression effect. The shear yield stress shows a linear growth trend with increased compressive yield stress. The shear yield stress under the compression-shear coupling effect is greater than that under the compression effect. The maximum shear yield stress is 349.24 Pa (flocculant dosage is 25 g t^{-1}), and the maximum shear yield stress is higher than that under compression effect. With the increase of shear yield stress, the concentration also shows a trend of rapid growth at first and then slow.

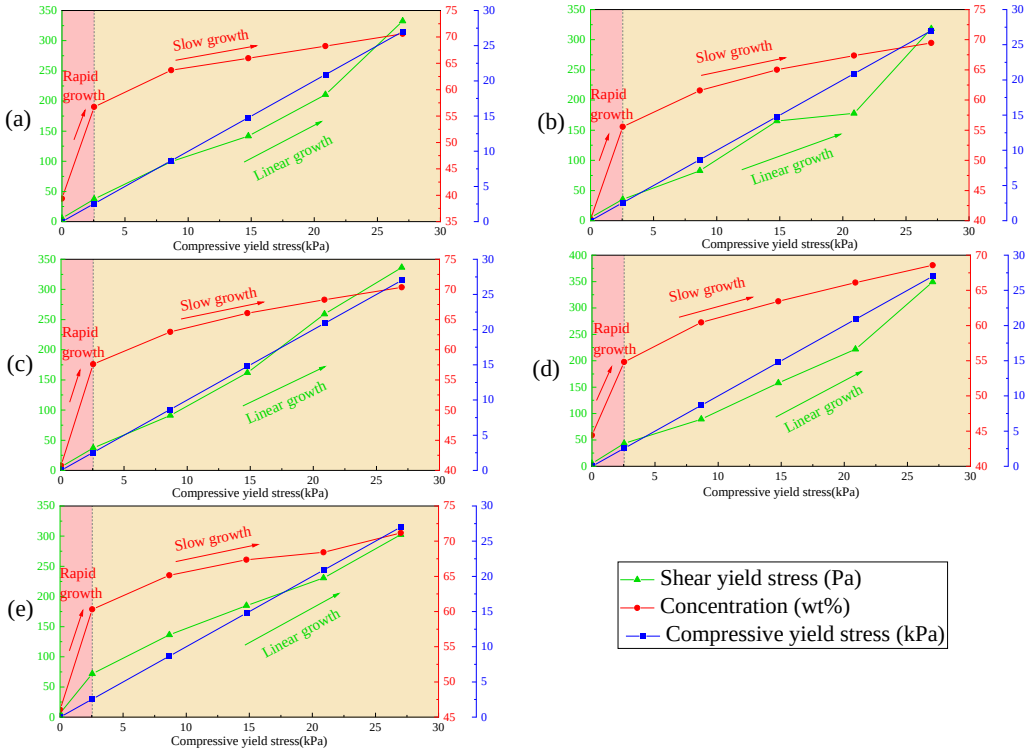

Fig. 5 Evolution of concentration-double yield stress under compression-shear coupling effect with different flocculant dosages: (a) 10 g t^{-1}; (b) 15 g t^{-1}; (c) 20 g t^{-1}; (d) 25 g t^{-1}; (e) 30 g t^{-1}

3.1.2 Evolution of concentration and rheological properties with different fine-grained tailings contents

The evolution of the concentration-double yield stress under compression effect with different fine-grained tailings contents is shown in Fig. 6. The concentrations of different fine-grained tailings contents increase rapidly at first and then slow down with the linear growth of compressive yield stress, and the growth rate (3.46, 3.21, 4.64, 3.41 and 3.96 %·kPa^{-1}) is higher in the low compressive yield stress range than that in the high compressive yield stress range (0.46, 0.52, 0.62, 0.63 and 0.57 %·kPa^{-1}). The maximum concentration corresponding to different fine-grained tailings content levels is 72.65, 69.86, 67.90, 62.81, and 60.26 wt%, respectively. It can be seen that with the growth of fine-grained tailings content, the concentration decreases. With the increase of compressive yield stress, shear yield stress shows a linear growth trend, and the maximum shear yield stress is 305.07 Pa (fine-grained tailings content is 20 wt%), and the concentration also shows a trend of rapid growth at first and then slow with the increase of shear yield stress.

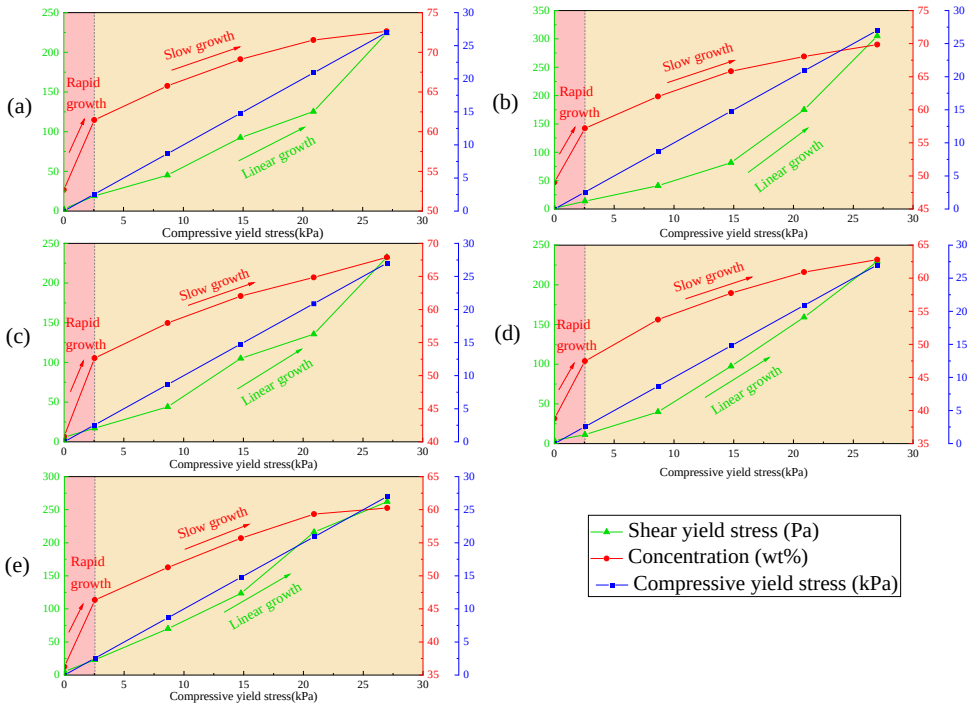

Fig. 6 Evolution of concentration-double yield stress under compression effect with different fine-grained tailings contents: (a) 10 wt%;(b) 20 wt%;(c) 30 wt%;(d) 40 wt%;(e) 50 wt%

Fig. 7 shows the evolution of the concentration-double yield stress under the compression-shear coupling effect with different fine-grained tailings contents. The concentrations of different fine-grained tailings contents increase rapidly at first and then slow down with the linear growth of compressive yield stress. The growth rate (4.15, 4.34, 6.59, 5.17, and 5.49 %·kPa^{-1}) in the low compressive yield stress range is higher than that (0.43, 0.46, 0.52, 0.52 %·kPa^{-1}) in the high compressive yield stress range. Moreover, the growth rate of concentration in the low compressive yield stress range under the compression-shear coupling effect is higher than that under the compression effect, but in the high compressive yield stress range, the opposite is true. The maximum concentrations corresponding to different fine-grained tailings contents are 73.71, 71.23, 70.35, 64.71, and 62.99 wt%, respectively. It can be seen that with the growth of fine-grained tailings content, the concentration decreases, and the concentration corresponding to different fine-grained tailings contents under the compression-shear coupling effect is higher than that under compression effect, which shows that the thickening effect under compression-shear coupling effect is better than that under compression effect. The shear yield stress shows a linear growth trend with increased compressive yield stress. The shear yield stress under the compression-shear coupling effect is greater than that under the compression. The maximum shear yield stress is 336.54 Pa (fine-grained tailings content is 30 wt%), and the maximum shear yield stress is higher than that under compression effect (growth ratio: 10.32%). With the increase of shear yield stress, the concentration also shows a trend of rapid growth at first and then slow.

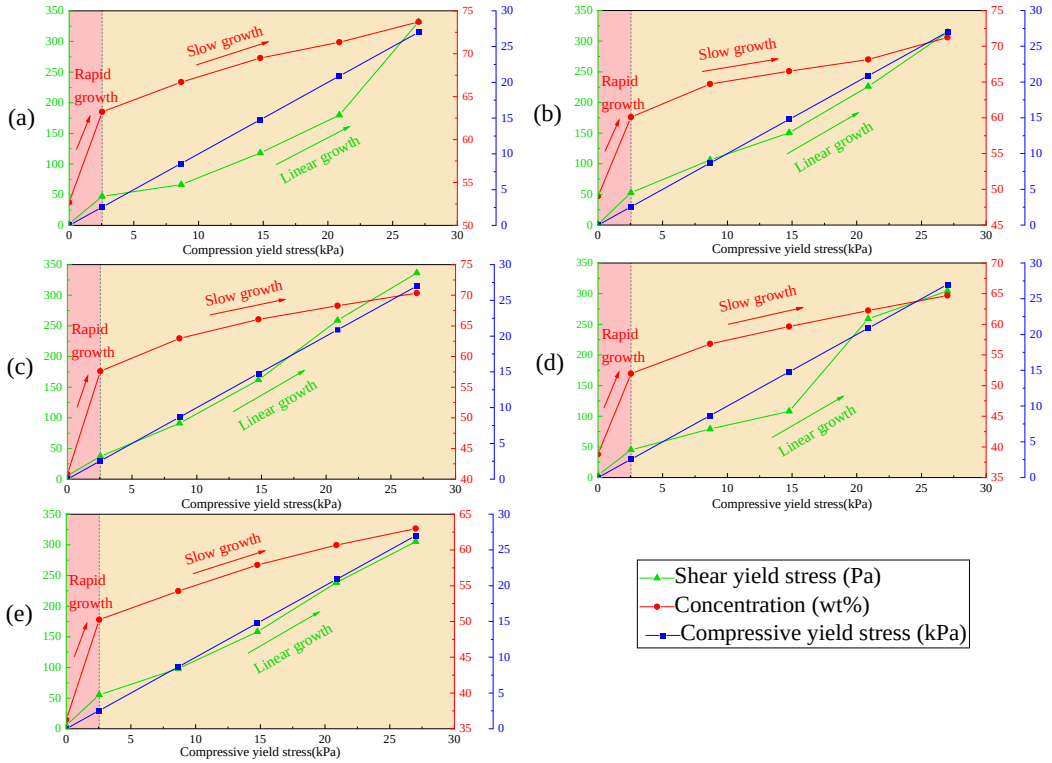

Fig. 7 Evolution of concentration-double yield stress under compression-shear coupling effect with different fine-grained tailings contents: (a) 10 wt%;(b) 20 wt%;(c) 30 wt%;(d) 40 wt%;(e) 50 wt%

3.2 Correlation analysis

3.2.1 Concentration-shear yield stress

The evolution of concentration and double yield stress in Section 3.1 shows that the concentration increases rapidly at first and then slowly with the linear growth of shear yield stress and compressive yield stress. The relationship between concentration, shear yield stress, and compressive yield stress under the compression and compression-shear coupling effects with different flocculant dosages and fine-grained tailings contents was characterized and analyzed, respectively. It is found that the relationship between concentration and shear yield stress and compressive yield stress is a power function, and the formulas are shown in Eq. (1) and Eq. (2).

$$U_{\text{Flocculant condition}} = m \cdot \tau^{n} \tag{1}$$

Where $U_{\text{Flocculant condition}}$ represents the concentration under different flocculant conditions, wt%; τ stands for the shear yield stress, Pa; m and n represent the fitting parameters.

$$U_{\text{Flocculant condition}} = a \cdot c^{b} \tag{2}$$

Where c stands for the compressive yield stress, kPa; a and b represent the fitting parameters.

Figures 8(a) and 8(b) show the fitting results of concentration-shear yield stress under compression effect and compression-shear coupling effect with different

flocculant dosages. The relationship between concentration and shear yield stress conforms to a power function. The R^2 values corresponding to each flocculant dosage level under the compression effect are 0.930, 0.936, 0.959, 0.987, and 0.962, respectively. The R^2 values under the compression-shear coupling effect are 0.967, 0.975, 0.962, 0.997, and 0.999, respectively, indicating that the fitting results are reliable.

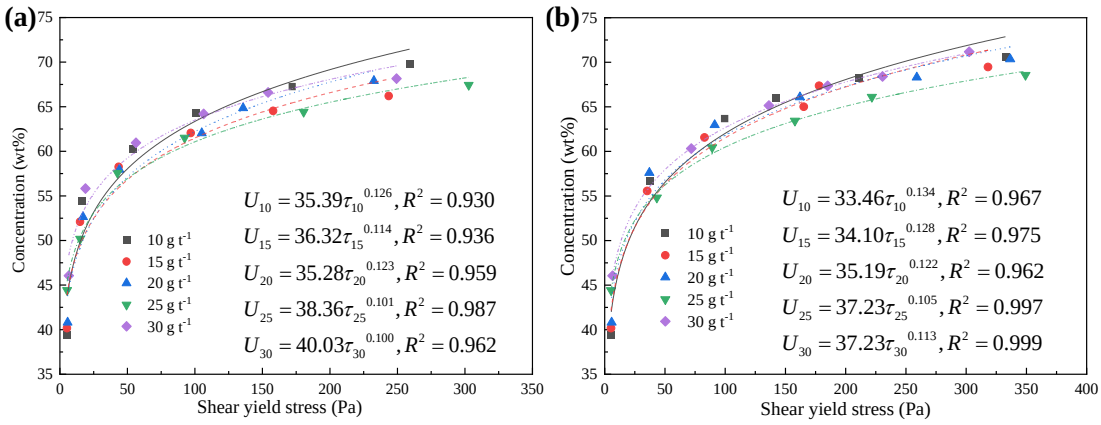

Fig. 8 Fitting results of concentration-shear yield stress under different flocculant dosages: (a) Compression effect; (b) Compression-shear coupling effect

Figures 9(a) and 9(b) show the fitting results of concentration-shear yield stress under the compression and compression-shear coupling effects with different fine-grained tailings contents. With the growth of fine-grained tailings content, the overall concentration curves decrease continuously, indicating that high fine-grained tailings content has an adverse effect on the concentration. The relationship between concentration and shear yield stress under compression effect and compression-shear coupling effect is a power function. The fitted R^2 values under the compression effect are 0.992, 0.993, 0.959, 0.979, and 0.990, respectively, and the fitted R^2 values under the compression-shear coupling effect are 0.990, 0.982, 0.962, and 0.990, respectively. Moreover, the fitting coefficient m of the Eq. (1) under the compression and compression-shear coupling effects decreases with the increase of fine-grained tailings content. The larger the fitting parameter m is, the better the thickening effect is, and the higher the concentration is. Hence, the concentration fitting curve shown in Figures 9(a) and 9(b) decreases with the increase of fine-grained tailings content.

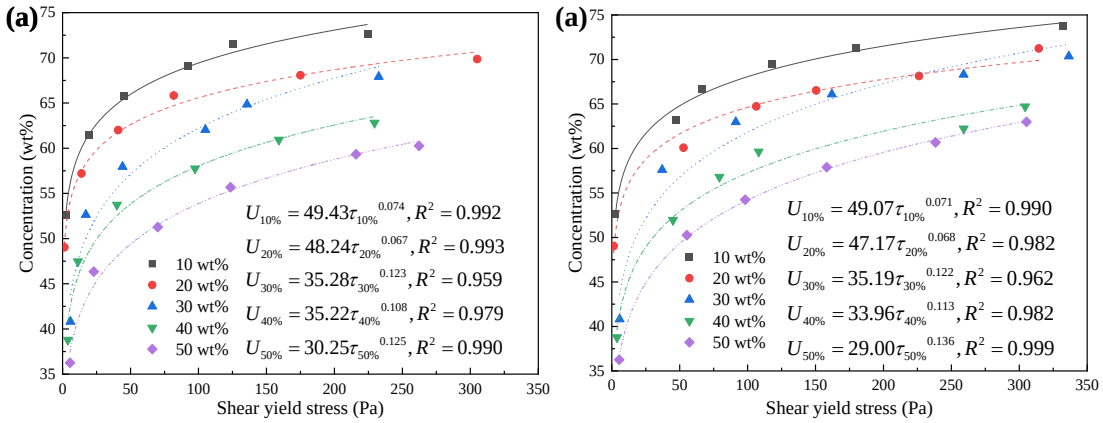

Fig. 9 Fitting results of concentration-shear yield stress under different fine-grained tailings contents: (a) Compression effect; (b) Compression-shear coupling effect

3.2.2 Concentration-compressive yield stress

Figures 10(a) and 10(b) show the fitting results of concentration-compressive yield stress under the compression and compression-shear coupling effects with different flocculant dosages. It can be seen from the figure that the relationship between concentration and compressive yield stress is a power function. The fitted R^2 values under the compression effect are 0.986, 0.997, 0.975, 0.994, and 0.993, respectively, and the fitted R^2 values under the compression-shear coupling effect are 0.994, 0.995, 0.992, 0.987, and 0.979, respectively.

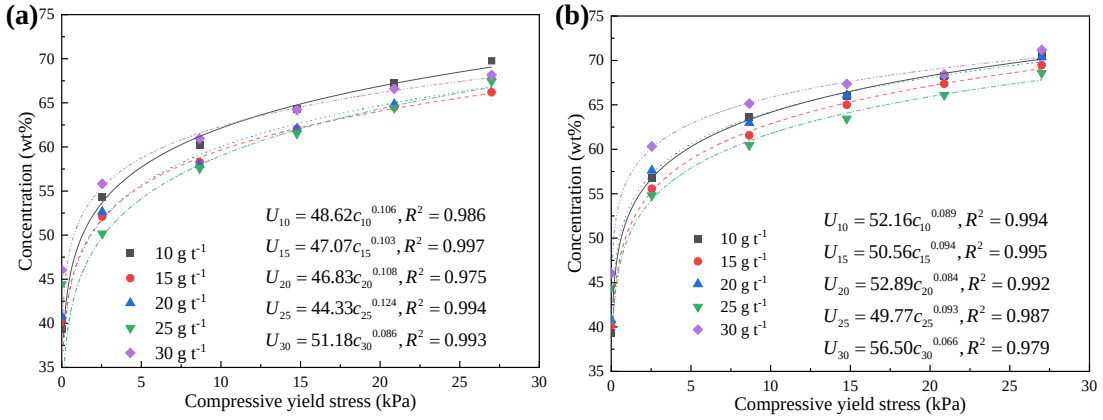

Fig. 10 Fitting results of concentration-compressive yield stress under different flocculant dosages: (a) Compression effect; (b) Compression-shear coupling effect

Figures 11(a) and 11(b) show the fitting results of concentration-compressive yield stress under the compression and compression-shear coupling effects with different fine-grained tailings contents. With the increase of fine-grained tailings content, the overall concentration curves move down continuously, indicating that high fine-grained tailings content has an adverse effect on the concentration. There is a power function relationship between concentration and compressive yield stress. The fitted R^2 values under the compression effect are 0.983, 0.986, 0.975, 0.992, and 0.974, respectively, and the fitted R^2 values under the compression-shear coupling effect are 0.960, 0.962, 0.992, and

0.974, respectively. Among them, the coefficient a of the fitting Eq. (2) under the compression and compression-shear coupling effects decreases with the increase of fine-grained tailings content, which shows again that the fine-grained tailings content has an adverse influence on the thickening effect, and the larger the fitting parameters a is, the better the thickening effect is and the higher the concentration is. Therefore, the concentration curve shown in Figures 11(a) and (b) decreases with the increase of fine-grained tailings content.

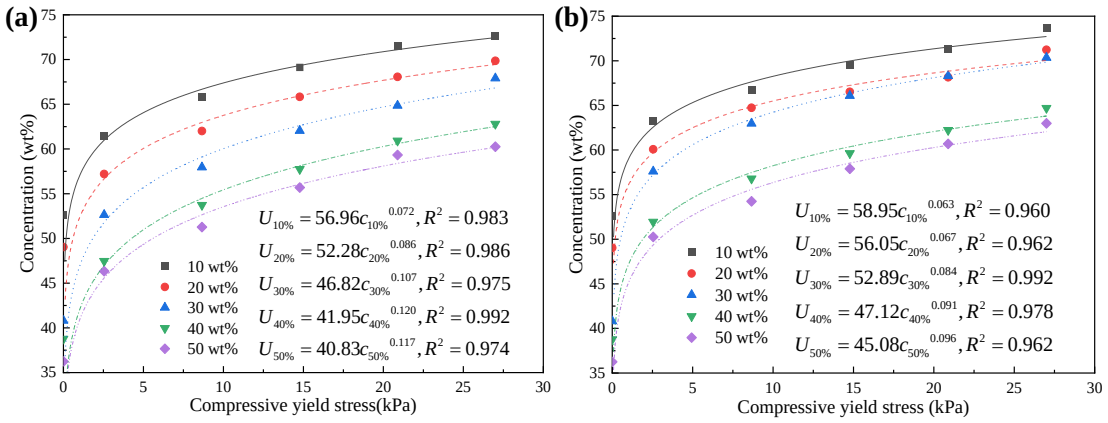

Fig. 11 Fitting results of concentration-compressive yield stress under different fine-grained tailings contents: (a) Compression effect; (b) Compression-shear coupling effect

3.2.3 Shear yield stress-compressive yield stress

A lot of research has been carried out to analyze the relationship between shear yield stress and compressive yield stress. Still, most of the research on thickened tailings is carried out under low compression stress (< 1 kPa), which is quite different from the high compression stress in industrial thickeners [23,29]. Therefore, studying the high compression stress of 0-30 kPa in this study is of great practical value. From the analysis in Section 3.1, it can be seen that there is a linear correlation between the shear yield stress and the compressive yield stress. Linear fitting (Eq. (3)) of shear yield stress-compressive yield stress under the compression and compression-shear coupling effects was carried out, respectively.

$$\tau = kc + p \tag{3}$$

Where k and p are the fitting parameters.

Fig. 12 shows the linear fitting results of shear yield stress-compressive yield stress under the compression and compression-shear coupling effects with different flocculant dosages. As shown in Fig. 12(a), the linear fitting R^2 values of different flocculant dosage levels under the compression effect are 0.967, 0.962, 0.955, 0.922, and 0.966, respectively. As shown in Fig. 12(b), under the compression-shear coupling effect, the linear fitting R^2 values of different flocculant dosages are 0.971, 0.952, 0.992, 0.973, and 0.978, respectively. The fitting effects are reliable.

A comparative analysis was conducted on the proportion coefficients (fitting line

slope k) of the fitting lines between shear yield stress and compressive yield stress under compression effect and compression-shear coupling effect, where the proportion coefficient represents the thickening rate of the thickened tailings. As shown in Fig. 13, the proportional coefficients of each flocculant dosage level under the compression effect are smaller than those under the compression-shear coupling effect, indicating that the thickening rate under compression-shear coupling effect is faster and the thickening effect is better, which is consistent with the fact that the concentration under compression-shear coupling effect is higher than that under compression effect.

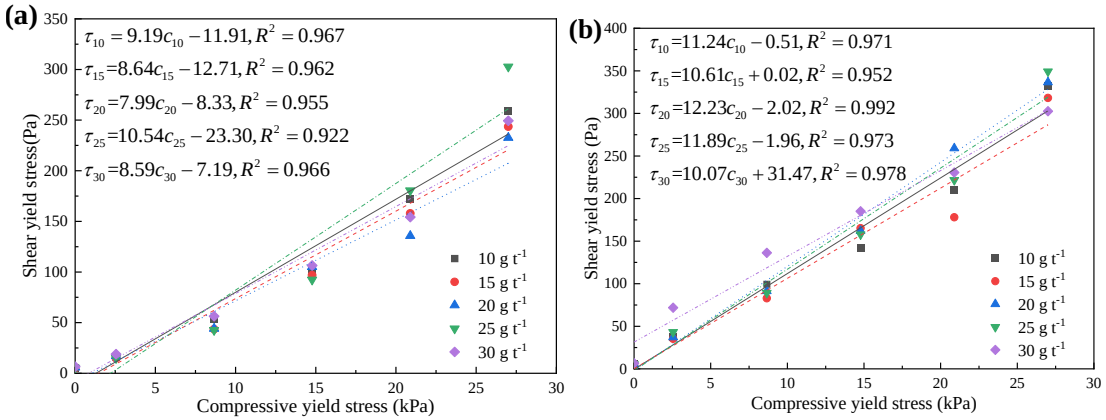

Fig. 12 Fitting results of shear yield stress-compressive yield stress with different flocculant dosages: (a) Compression; (b)Compression-shear coupling

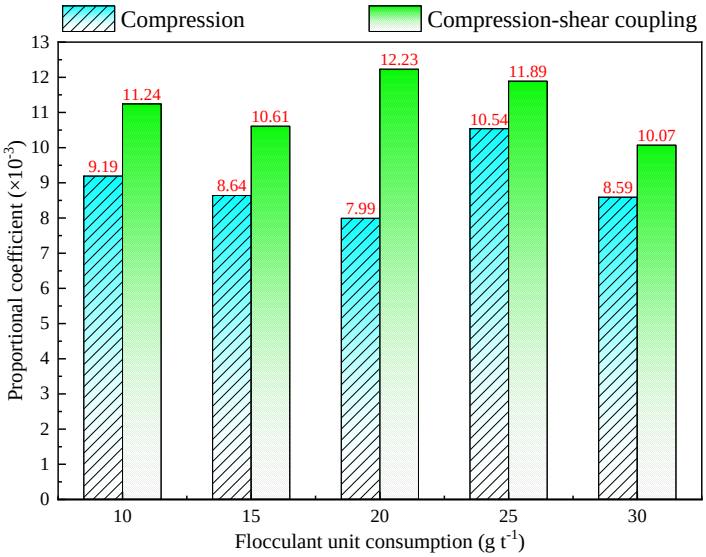

Fig. 13 Comparative analysis of the proportional coefficients of the shear yield stress-compressive yield stress fitting lines under compression and compression-shear coupling effects with different flocculant dosages

Fig. 14 shows the linear fitting results of shear yield stress-compressive yield stress under the compression and compression-shear coupling effects with different fine-grained tailings contents. As shown in Fig. 14(a), the linear fitting R^2 values of different fine-grained tailings contents under the compression effect are 0.945, 0.908, 0.955, 0.940, and 0.986, respectively. As shown in Fig.

14(b), under the compression-shear coupling effect, the linear fitting R^2 values of different fine-grained tailings contents are 0.913, 0.986, 0.992, 0.940, and 0.992, respectively, and the fitting effects are reliable. The proportional coefficients of shear yield stress-compressive yield stress fitting lines under compression and compression-shear coupling effects were compared and analyzed in Fig. 15. The proportional coefficients of each fine-grained tailings content level under compression effect are all lower than those under compression-shear coupling effect, which once again shows that the thickening rate is faster and the thickening effect is better, and it is also verified that the concentration under compression-shear coupling effect is higher than that under compression effect.

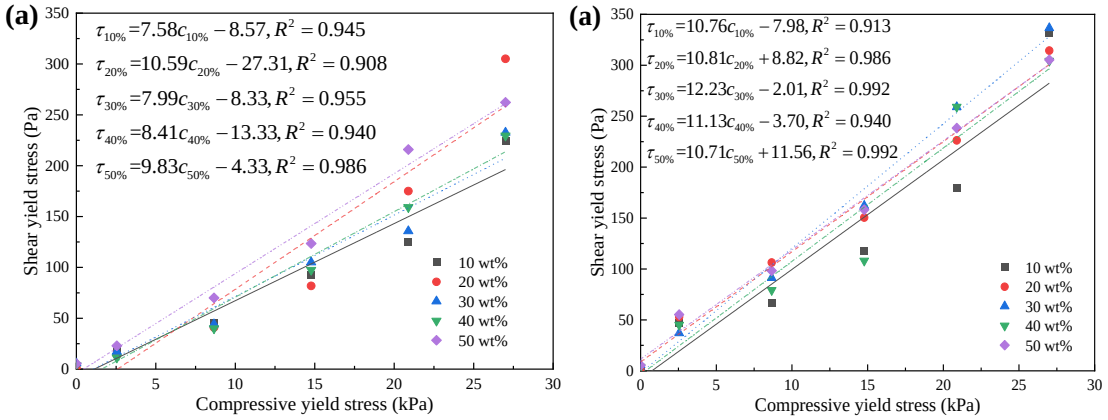

Fig. 14 Fitting results of shear yield stress-compressive yield stress with different fine-grained tailings contents: (a) Compression effect; (b) Compression-shear coupling effect

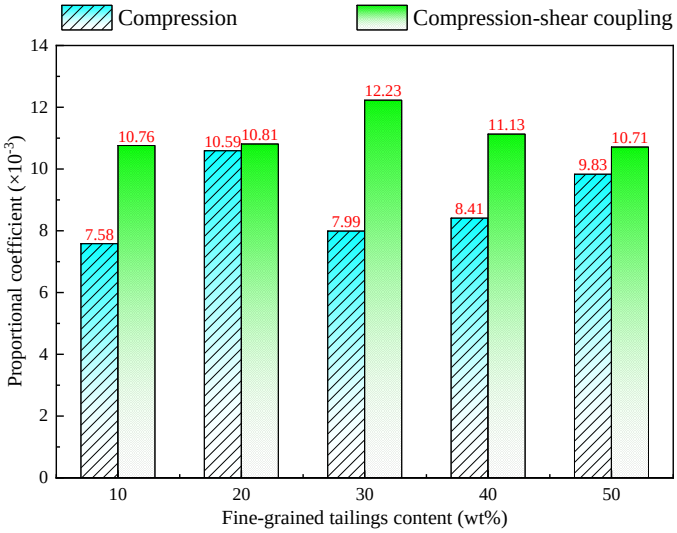

Fig. 15 Comparative analysis of the proportional coefficients of the shear yield stress-compressive yield stress fitting lines under compression and compression-shear coupling effects with different fine-grained tailings contents

3.3 Thickening mechanism

In this study, the compressive yield stress range of the experiment is divided into two stages, namely, low compression stress range and high compression stress range. Among them, the low compression stress range is 0-2.55 kPa,

and the high compression stress range is 8.66-27 kPa. The low compression stress range is consistent with the compression stress range of the indoor thickening experiments, and the high compression stress range is consistent with the high mud layer pressure in the industrial thickeners. The evolution of shear yield stress and compressive yield stress in low and high compression stress ranges under the compression and compression-shear coupling effects with different flocculant dosages and fine-grained tailings contents were fitted, respectively. The corresponding proportional coefficients of low and high compression stress ranges are obtained and compared to reveal the thickening mechanism.

3.3.1 Thickening mechanism under compression

As shown in Figures 16(a) and 16(b), they are the fitting results of low and high compression stress ranges under the compression effect with different flocculant dosages and fine-grained tailings contents. It can be seen that the slopes of the fitting straight lines in the low compression stress range are lower than that in the high compression stress range, indicating that under compression effect, the thickening rate in the low compression stress range is lower than that in the high compression stress range.

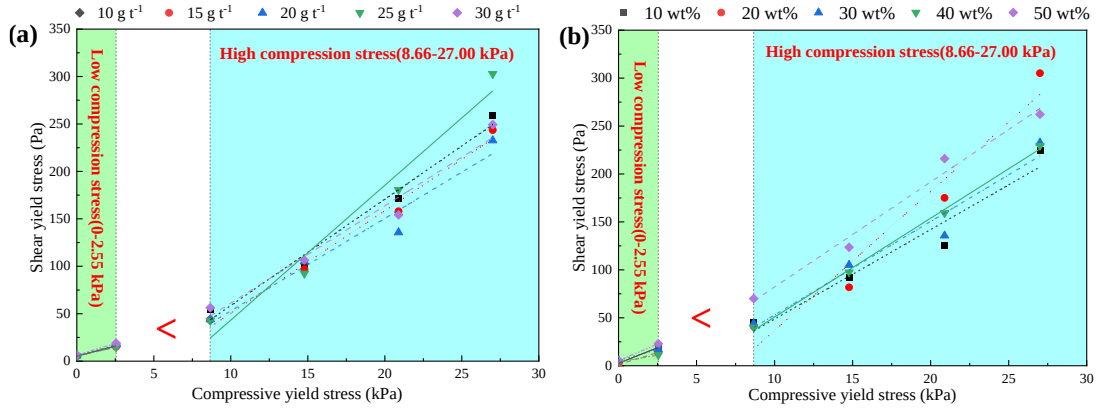

Fig. 16 Comparison of proportional coefficients between low and high compression stress ranges under compression effect: (a) Flocculant dosage; (b) Fine-grained tailings content.

From the comparative analysis of the proportional coefficients of the low and the high compression stress ranges shown in Figures 17(a) and 17(b), it can also be seen that the proportional coefficients of the high compression stress range corresponding to different flocculant dosages and fine-grained tailings contents are higher than those in the low compression stress range.

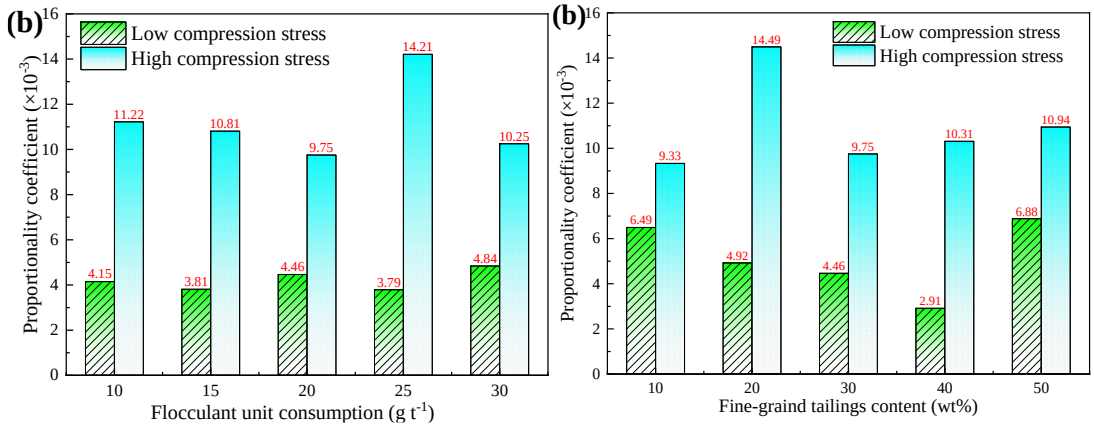

Fig. 17 Comparison of k values between low and high compression stress ranges under compression effect: (a) Flocculant dosage; (b) Fine-grained tailings content

The thickening process of thickened tailings is accompanied by the evolution of flocs structure and the drainage channels, which is the important internal mechanism causing the evolution of double yield stress [43,48]. The evolution of flocs mainly manifests as their rupture and reconstruction, releasing the stored water in the flocs [43]. The evolution of drainage channels is mainly through increasing the connectivity of channels. The water between flocs is discharged to the solid-liquid separation interface [49-51].

As shown in Fig. 18, in the initial state of the thickened tailings, the tailings floc size is the largest, the floc arrangement is disordered, the drainage channels are in low quantity, the connectivity is low, most of the channels are blocked, and there is a large amount of water between and inside the flocs, the concentration and shear yield stress are low. Under the low compression stress range (Fig. 18(a)), the tailings flocs partially rupture and reconstruct at the top of the thickened tailings. However, most of the flocs remain in the original state at the bottom of the thickened tailings. Because there is a large amount of water between and inside the flocs, the shear resistance is weak, and the shear yield stress increases slowly. Under the high compression stress range, flocs undergo large-scale rupture and reconstruction, and flocs are in a disordered arrangement, drainage channels decrease, channels close, connectivity decreases, thickening effect is poor, and the shear resistance of thickened tailings is enhanced due to the decrease of water content between and inside flocs. Moreover, the growth rate of shear yield stress increases (Fig. 18(c)).

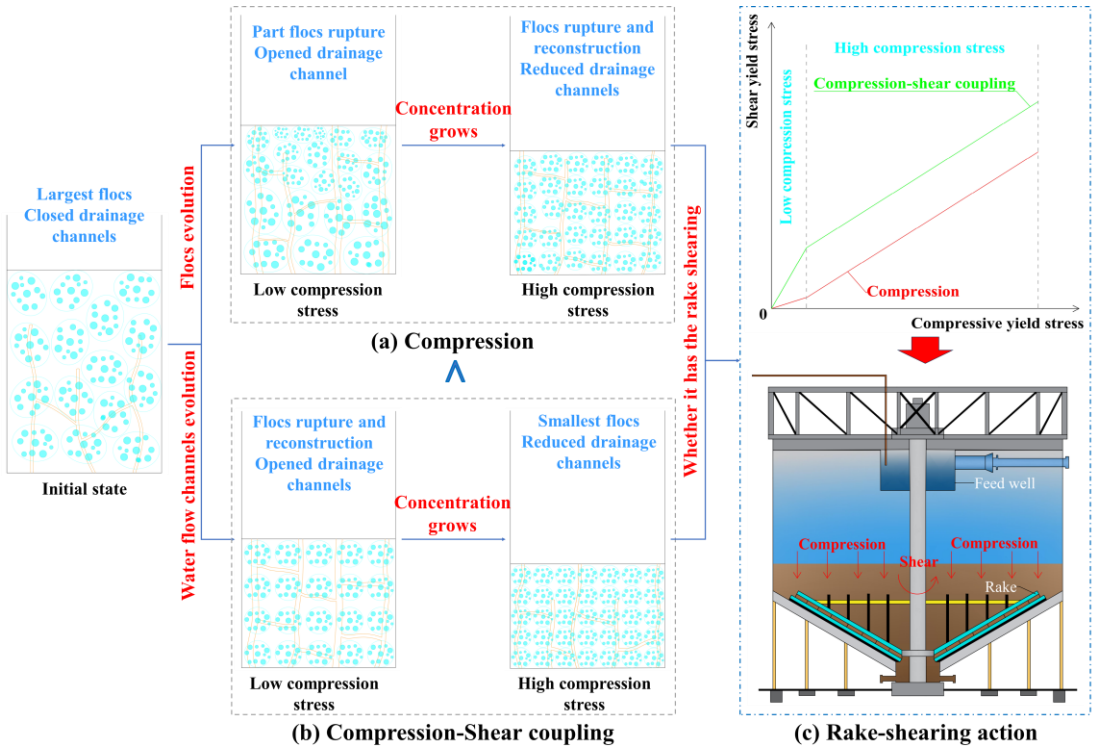

Fig. 18 Influence of floc structure and drainage channel evolutions on thickening process

3.3.2 Thickening mechanism under compression-shear coupling

As shown in Figures 19(a) and 19(b), they are the fitting results of low and high compression stress ranges under the compression-shear coupling effect under different flocculant dosages and fine-grained tailings contents. It can be seen that the slopes of the fitting straight lines in the low compression stress range are obviously higher than that in the high compression stress range, indicating that under the compression-shear coupling effect, the thickening rate in the low compression stress range is higher than that in the high compression stress range, thereby improving the overall thickening effect. This also confirms that the thickening effect of the compression shear coupling effect is better than that of the compression effect.

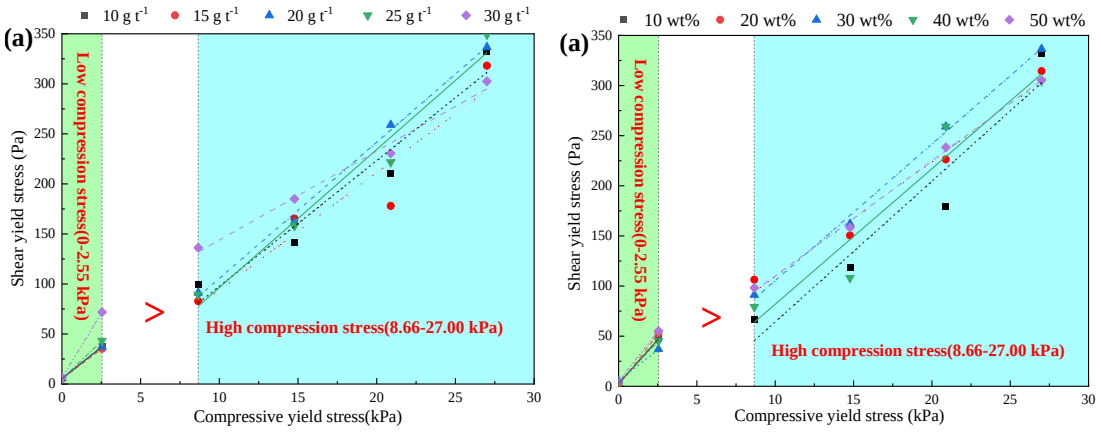

Fig. 19 Comparison of proportional coefficients between low and high compression stress ranges under compression-shear coupling effect: (a) Flocculant dosage; (b) Fine-grained tailings content

From the comparative analysis of the proportional coefficients of the low and the high compression stress ranges shown in Figures 20(a) and 20(b), it can also be seen that the proportional coefficients of the high compression stress range corresponding to different flocculant dosages and fine-grained tailings contents are mostly lower than those in the low compression stress range. It shows that the thickening rate in the low compression stress range is higher than that in the high compression stress range. Moreover, the proportion coefficients in the low compression stress range under the compression-shear coupling effect are much higher than those under the compression effect, and the proportion coefficients in the high compression stress range are roughly similar in both thickening conditions. Corresponding to the proportional coefficients of shear yield stress-compressive yield stress under the compression-shear coupling effect (Fig. 12 and Fig. 14), it also shows that the thickening rate under the compression-shear coupling effect is higher, which verifies the conclusion that the concentration under compression-shear coupling effect is higher than that under compression effect.

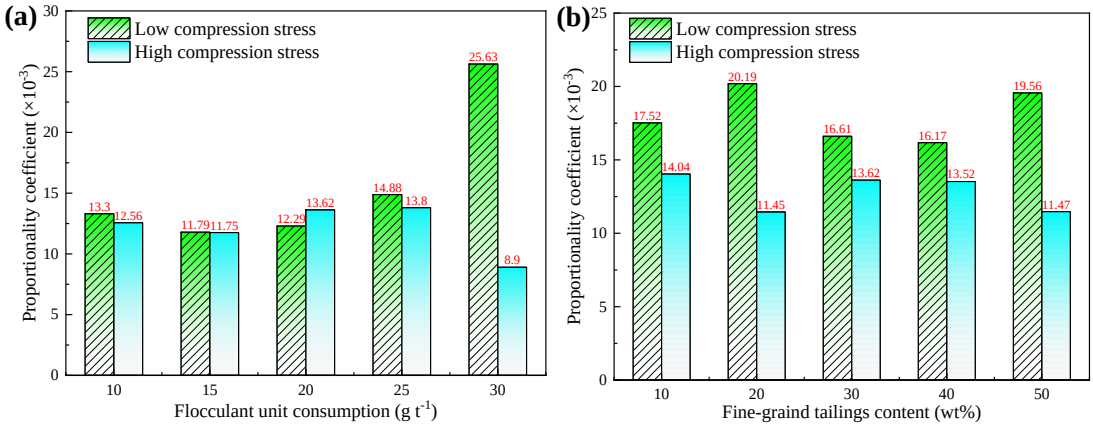

Fig. 20 Comparison of k values between low and high compression stress ranges under compression-shear coupling effect: (a) Flocculant dosage; (b) Fine-grained tailings content

As shown in Fig. 18(b), under the compression-shear coupling effect, many flocs break under the lower compression stress acts on the thickened tailings. The rake-shearing action will cause flocs to rearrange. Meanwhile, it also promotes the opening of the drainage channels. The channel size is large, the connectivity is high, the thickening effect is good, the flocs structure is compact, and the water between and inside the flocs is discharged with the drainage channels. Compared with the compression effect, the concentration increases more rapidly. Due to the large amount of water discharged between and inside the flocs, the shear resistance is enhanced, and the shear yield stress also increases fast. In the higher compression stress range, the tailings floc ruptures and restructures under rake-shearing and finally forms the smallest floc size and the largest floc quantity. Due to the further discharge of water between flocs, the structure is compact, the quantity of the drainage channels reduces, the connectivity decreases, the thickening rate decreases. Furthermore, the shear resistance changes little, and the shear yield stress increases at a lower rate

(Fig. 18(c)) compared to the low compression stress range.

3.3.3 Comparison of thickening mechanisms between compression and compression-shear coupling effects

According to the comparative analysis of the proportional coefficients of shear yield stress-compressive yield stress in the low and high compression stress ranges in Sections 3.3.1 and 3.3.2, it can be seen that compared with the compression effect, the compression-shear coupling effect greatly improves the thickening rate and thickening effect in the low compression stress range by introducing the rake-shearing action. The concentration growth ratio varies with different compression stresses. Therefore, the growth ratios of concentration corresponding to different compression stresses are also an important factor to measure the thickening mechanism. The thickening mechanism was further verified by the growth ratio of concentration. The growth ratios of concentration with different compressive yield stresses under compression and compression-shear coupling effects with varying flocculant dosages of and fine-grained tailings contents were analyzed, respectively.

According to the growth ratios of concentration, the three-dimensional distribution diagrams of concentration growth ratio are shown in Figures 21(a) and 21(b). Under the high compressive yield stress of 8.66, 14.78, 20.89, and 27.00 kPa, there is no significant difference in the growth ratio of concentration, which is all less than 0.15. The main difference occurs at a low compressive yield stress of 2.55 kPa. As can be seen from Fig. 21, there is a large difference between the growth ratio of concentration under the compression-shear coupling effect and compression effect corresponding to 2.55 kPa, and the growth ratios of concentration under compression-shear coupling effect are significantly higher than that under the compression effect. It is verified that the thickening rate and effect in the low compression stress range are greatly improved by the introduction of rake-shearing action under the compression-shear coupling effect, and the thickening mechanism that the concentration under the compression-shear coupling effect is higher than that under the compression effect is also revealed (Fig. 18(c)). Therefore, it is suggested to adopt the deep-cone structure with high mud layer pressure and the rake-shearing structure for industrial thickeners.

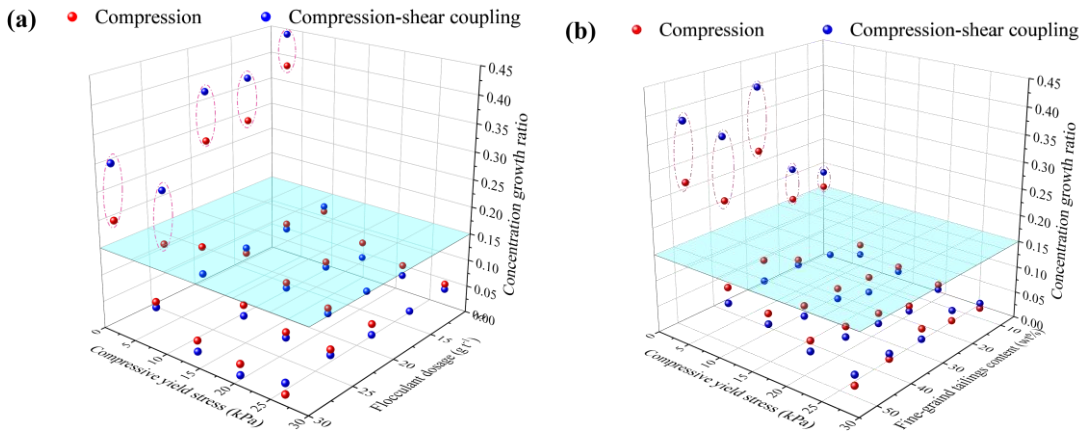

Fig. 21 Distribution diagram of concentration growth ratio under compression effect and compression-shear coupling effect: (a) Flocculant dosage; (b) Fine-grained tailings content

4 Conclusion

In this study, the rheological properties and concentration of thickened tailings under compression and compressed-shear coupling effects were tested with different flocculant dosages and fine-grained tailings contents. Concentration-double yield stress correlation analysis, and thickening mechanism analysis were carried out. The main conclusions are as follows:

(1) The concentration increases rapidly in the low compression stress range and slowly in the high compression stress range with the linear growth of compressive yield stress and shear yield stress, and the concentration under the compression-shear coupling effect is higher than that under the compression effect. The higher the fine-grained tailings content, the lower the concentration. The shear yield stress increases linearly with the growth of compressive yield stress.

(2) There is a power function relationship between concentration and shear yield stress and compressive yield stress, respectively. The fitting curves under different fine-grained tailings contents move down with the increase of fine-grained tailings content.

(3) The linear fitting of the relationship under each experimental factor shows that the proportional coefficients under the compression effect are smaller than that under the compression-shear coupling effect, indicating that the thickening rate is higher and the thickening effect is better under the compressor-shear coupling effect.

(4) The thickening mechanism was analyzed from the perspective of the double yield stress relationship and evolution of flocs and drainage channels. The thickening rate in the low compression stress range under compression is higher than that in the high compression stress range, but under the compression-shear coupling effect, this phenomenon is the opposite.

(5) The concentration growth ratio shows that the difference of concentration growth ratio between the compression effect and compressor-shear coupling effect is mainly concentrated in the low compression stress range of 0-2.55kPa, indicating that compared with a compression effect, the introduction of rake-

shearing action under compression-shear coupling effect mainly increases the thickening rate in the low compression stress range, and then increases the overall thickening effect, revealing the thickening mechanism with higher concentration under the compression-shear coupling effect.

Acknowledgment

This work was funded by the National Natural Science Foundation of China (no. 52130404, 52304121), the Fundamental Research Funds for the Central Universities (no.FRF-TP-22-112A1), Guangdong Basic and Applied Basic Research Foundation (no. 2021A1515110161), ANID (Chile) through Fondecyt project 1210610, Centro de Modelamiento Matemático (BASAL funds for Centers of Excellence FB210005), CRHIAM project ANID/FONDAP/15130015, and Anillo project ANID/ACT210030.

Conflict of Interest

The authors declare no conflict of interest.

References

[1] Menglong Wu, Yicheng Ye, Nanyan Hu, Qihu Wang, Wenkan Tan. Scientometric analysis on the review research evolution of tailings dam failure disasters. Environmental Science and Pollution Research. 2023, 30: 13945–13959.

[2] Yong Wang, Zhenqi Wang, Aixiang Wu, Liang Wang, Qing Na, Chen Cao, Gangfeng Yang. Experimental research and numerical simulation of the multi-field performance of cemented paste backfill: Review and future perspectives. International Journal of Minerals Metallurgy and Materials. 2023, 30(2):193-208.

[3] Dylan D. Furszyfer Del Rio, Benjamin K. Sovacool, Aoife M. Foley, Steve Griffiths, Morgan Bazilian, Jinsoo Kim, David Rooney. Decarbonizing the glass industry: A critical and systematic review of developments, sociotechnical systems and policy options. Renewable and Sustainable Energy Reviews. 2022, 155.

[4] Mansour Edraki, Thomas Baumgartl, Emmanuel Manlapig, Dee Bradshaw, Daniel M. Franks, Chris J. Moran. Designing mine tailings for better environmental, social and economic outcomes: a review of alternative approaches. Journal of Cleaner Production. 2014, 84: 411-420.

[5] You Zheng, Jianzhong Xiao, Jinhua Cheng. Industrial Structure Adjustment and Regional Green Development from the Perspective of Mineral Resource Security. International Journal of Environmental Research and Public Health. 2020, 17(19).

[6] Aixiang Wu, Zhuen Ruan, Jiandong Wang, Rheological behavior of paste in metal mines, Int J Miner Metall Mater, 2022, 29: 717–726.

[7] Chongchong Qi, Andy Fourie. Cemented paste backfill for mineral tailings management: Review and future perspectives. Minerals Engineering. 2019, 144.

[8] Zhenqi Wang, Yong Wang, Liang Cui, Cheng Bi, Aixiang Wu. Insight into the isothermal multiphysics processes in cemented paste backfill: Effect of curing time and cement-to-tailings ratio. Construction and Building Materials.

2022, 235.
[9] Shan Gao, Wei Li, Kekuo Yuan, Chuanxin Rong. Properties and application of thixotropic cement paste backfill with molybdenum tailings. Journal of Cleaner Production. 2023, 391.
[10] Xiaoyan Zhang, Muyan Xu, Lang Liu, Chao Huan, Yujiao Zhao, Chongc hong Qi, KI-IL Song. Experimental study on thermal and mechanical properties of cemented paste backfill with phase change material. Journal of Materials Research and Technology. 2020, 9(2): 2164-2175.
[11] Huazhe Jiao, Shufei Wang, Yixuan Yang, Xinming Chen. Water recovery improvement by shearing of gravity-thickened tailings for cemented paste backfill. Journal of Cleaner Production. 2020, 245.
[12] Liuhua Yang, Jincang Li, Hongbin Liu, Huazhe Jiao, Shenghua Yin, Xinming Chen, Yang Yu. Systematic review of mixing technology for recycling waste tailings as cemented paste backfill in mines in China. International Journal of Minerals Metallurgy and Materials. 2023, 30: 1430–1443.
[13] Haiyong Cheng, Shunchuan Wu, Hong Li, Xiaoqiang Zhang. Influence of time and temperature on rheology and flow performance of cemented paste backfill. Construction and Building Materials. 2020, 231.
[14] Lang Liu, Chao Zhu, Chongchong Qi, Mei Wang, Chao Huan, Bo Zhang, KI-IL Song. Effects of curing time and ice-to-water ratio on performance of cemented paste backfill containing ice slag. Construction and Building Materials, 2019, 228.
[15] Coe H S, Clevenger G H. Methods for determining the capacity of slime settling tanks. Traps. A1ME. 1916, 55: 356-385.
[16] Kynch G J. A theory of sedimentation. Traps Faraday Soc. 1952, 48(2): 166-176.
[17] Liyi Zhu, Wensheng Lyu, Peng Yang, Zhikai Wan. Effect of ultrasound on the flocculation-sedimentation and thickening of unclassified tailings. Ultrasonics Sonochemistry. 2020, 66.
[18] Qiuyi Lu, Bin Yan, Lei Xie, Jun Huang, Yang Liu, Hongbo Zeng. A two-step flocculation process on oil sands tailings treatment using oppositely charged polymer flocculants. Science of The Total Environment. 2016, 565: 369-375.
[19] Lianfu Zhang, Hongjiang Wang, Aixiang Wu, Bern Klein. Predicting beach profiles for thickened tailings surface deposition. Minerals Engineering. 2023, 201.
[20] R. Arjmand, M. Massinaei, A. Behnamfard. Improving flocculation and dewatering performance of iron tailings thickeners. Journal of Water Process Engineering. 2019, 31.
[21] Weicheng Ren, Rugao Gao, Youzhi Zhang, Maoxin Hou. Rheological Properties of Ultra-Fine Tailings Cemented Paste Backfill under Ultrasonic Wave Action. Minerals. 2021, 11(7).
[22] Claudia Castillo, Christian F. Ihle, Ricardo I. Jeldres. Chemometric

770 Optimisation of a Copper Sulphide Tailings Flocculation Process in the
771 Presence of Clays. Minerals. 2019, 9(10).
772 [23] Xuetao Wang, Baoyu Cui, Dezhou Wei, Zhenguo Song, Yi He, Andrew E.
773 Bayly. CFD-PBM modelling of tailings flocculation in a lab-scale gravity
774 thickener. Powder Technology. 2022, 396: 139-151.
775 [24] Mohammed Derqaoui, Imane Aarab, Abdelmoughit Abidi, Abdelrani
776 Yaacoubi, Khalid El Amari, Abderahman Etahiri, Abdelaziz Baçaoui. The effect
777 of calcium ions on the flotation behavior of fluorapatite. Mineral Processing and
778 Extractive Metallurgy Review. 2022, 1-10.
779 [25] Juan I. Langlois, Aldo Cipriano. Dynamic modeling and simulation of
780 tailing thickener units for the development of control strategies. Minerals
781 Engineering. 2019, 131: 131-139.
782 [26] Chenyu Fang, Dakuo He, Kang Li, Yan Liu, Fuli Wang. Image-based
783 thickener mud layer height prediction with attention mechanism-based CNN.
784 ISA Transactions. 2022, 128: 677-689
785 [27] . Rudman, K. Simic, D.A. Paterson, P. Strode, A. Brent, I.D. Šutalo. Raking
786 in gravity thickeners. International Journal of Mineral Processing. 2008, 86: 114-
787 130.
788 [28] M. Rudman, D.A. Paterson, K. Simic. Efficiency of raking in gravity
789 thickeners. International Journal of Mineral Processing. 2010, 95: 30-39.
790 [29] J.B Farrow, R.R.M Johnston, K Simic, J.D Swift. Consolidation and
791 aggregate densification during gravity thickening. Chemical Engineering
792 Journal. 2000, 80: 141-148.
793 [30] Jinglong Gao, Andy Fourie. Using the flume test for yield stress
794 measurement of thickened tailings. Minerals Engineering. 2015, 81:116-127.
795 [31] S KY Gawu and A B Fourie. Assessment of the modified slump test as a
796 measure of the yield stress of high-density thickened tailings. Canadian
797 Geotechnical Journal. 2011, 41(1): 39-47.
798 [32] Shabnam Mizani, Paul Simms. Method-dependent variation of yield
799 stress in a thickened gold tailings explained using a structure based viscosity
800 model. Minerals Engineering. 2016, 98: 40-48.
801 [33] Yong Wang, Aixiang Wu, Zhuen Ruan, Zhihui Wang, Zongsu Wei,
802 Gangfeng Yang, Yiming Wang. Reconstructed rheometer for direct monitoring
803 of dewatering performance and torque in tailings thickening process.
804 International Journal of Minerals Metallurgy and Materials. 2020, 27: 1430–
805 1437.
806 [34] Zhuen Ruan, Aixiang Wu, Raimund Bürger, Fernando Betancourt, Yiming
807 Wang, Yong Wang, Huazhe Jiao, Shengkai Wang. Effect of interparticle
808 interactions on the yield stress of thickened flocculated copper mineral tailings
809 slurry. Powder Technology. 2021, 392: 278-285.
810 [35] David V. Boger. Rheology and the resource industries. Chemical
811 Engineering Science. 2009, 64(22): 4525-4536.
812 [36] K. El Mahboub, M. Mbonimpa, T. Belem, A. Maqsoud. Rheological

characterization of cemented paste backfills containing superabsorbent polymers (SAPs). Construction and Building Materials. 2022, 317.

[37] Matías. Jeldres, Norman Toro, Sandra Gallegos, Pedro Robles, Iván Salazar, Phillip D. Fawell, Ricardo I. Jeldres. Reducing Magnesium within Seawater Used in Mineral Processing to Improve Water Recovery and Rheological Properties When Dewatering Clay-Based Tailings. Polymers. 2022, 14(2).

[38] Rachel Bryan, Paul Simms, Rens Verburg. Coupling oxidation to transient drying during multilayer deposition of thickened gold tailings. Minerals Engineering. 2010, 23(14): 1101-1112.

[39] Shi Wang, Xuepeng Song, Xiaojun Wang, Qiusong Chen, Jianchun Qin, Yuxian Ke. Influence of coarse tailings on flocculation settlement. International Journal of Minerals Metallurgy and Materials. 2020,27: 1065–1074.

[40] Shenghua Yin, Yongqiang Hou, Shixing Yang, Xin Chen. Study on static and dynamic flocculation settlement characteristics of fine tailings slurry and influence of flocculant on strength of fine tailings backfill. Case Studies in Construction Materials. 2022, 17.

[41] Mehdi Rahimi, Ali A. Abdollahzadeh, Bahram Rezai. Dynamic simulation of tailing thickener at the Tabas coal washing plant using the phenomenological model. International Journal of Mineral Processing. 2016, 154: 35-40.

[42] Michael R. MacIver, Marek Pawlik. A floc structure perspective on sediment consolidation in thickened tailings. Chemical Engineering Science. 2202, 263.

[43] Philip Ofori, Anh V. Nguyen, Bruce Firth, Clint McNally, Orhan Ozdemir. Shear-induced floc structure changes for enhanced dewatering of coal preparation plant tailings. Chemical Engineering Journal. 2011, 172: 914-923.

[44] Dan Zhang, Tinu Abraham, Trong Dang-Vu, Jonathan Xu, Sarang P. Gumfekar, Thomas Thundat. Optimal floc structure for effective dewatering of polymer treated oil sands tailings. Minerals Engineering. 2021,160.

[45] Di Zheng, Weidong Song, Yuye Tan, Shuai Cao, Zilong Yang, Lijuan Sun. Fractal and microscopic quantitative characterization of unclassified tailings flocs. International Journal of Minerals Metallurgy and Materials. 2021, 28: 1429–1439.

[46] Huazhe Jiao, Wenbo Yang, Zhu'en Ruan, Jianxin Yu, Juanhong Liu, Yixuan Yang. Microscale mechanism of tailing thickening in metal mines. International Journal of Minerals Metallurgy and Materials. 2023, 30: 1538–154.

[47] Vold M J. Computer simulation of floc formation in a colloidal suspension. Journal of Colloid Science. 1963, 7: 684-695.

[48] Huazhe Jiao, Wenxiang Zhang, Yixuan Yang, Liuhua Yang, Kaijian Hu, Jianxin Yu. Pore Structure Evolution and Seepage Characteristics in Unclassified Tailing Thickening Process. Minerals. 2022, 12(2).

[49] Gezhong Chen, Cuiping Li, Zhuen Ruan, Raimund Bürger, Yuan Gao, Hezi Hou, Structural evolution of bed drainage channels under the shear effect

of the whole process of tailings thickening, Minerals Engineering, 2023, 203.
[50] Xinming Chen, Xiangfei Jin, Huazhe Jiao, Yixuan Yang, Juanhong Liu. Pore Connectivity and Dewatering Mechanism of Tailings Bed in Raking Deep-Cone Thickener Process. Minerals. 2020, 10(4).
[51] Gezhong Chen, Cuiping Li, Zhuen Ruan, Raimund Bürger, Hezi Hou, Research on floc structure and physical properties based on pipeline flocculation, Journal of Water Process Engineering, 2023, 53.